The Influence of Tensile Stress States on the Failure of HY-100 Steel

D.M. GOTO, D.A. KOSS, and V. JABLOKOV

The failure of an HY-100 steel plate has been examined as a function of stress state using notched and un-notched axisymmetric tensile specimens. The results show that increasing stress triaxiality leads to a rapid decrease in failure strains in a manner that is exponentially dependent on the degree of triaxiality. Two ductile failure mechanisms are identified: a void coalescence process, in which relatively equiaxed voids grow to impingement, and a void-sheet process, which links by a shear instability process large, elongated inclusion-initiated voids. The void-sheet mechanism intervenes and limits ductility at high-stress triaxialities in transversely oriented HY steel plate material, whereas the former process controls failure in longitudinally oriented material. These orientation effects are related to the morphology and alignment of the nonmetallic inclusion stringers that act as the primary void nucleation sites. Calcium treatments for inclusion-shape control improve ductility, especially at intermediate-stress triaxialities, primarily by suppressing the local conditions which give rise to the void-sheet instability process.

I. INTRODUCTION

PREDICTING the ductile failure of structures subjected to multiaxial stress states requires modeling and simulation. However, the failure prediction of structures manufactured of high-toughness steels, such as are used in Navy ship hulls, cannot be made solely by employing either linear or nonlinear fracture mechanics. A local-fracture approach is often necessary, which defines local fracture conditions by an appropriate failure criterion.[1–5] For example, a criterion based on the equivalent strain to failure, which is sensitive to the hydrostatic tensile stress, is usually prescribed and expressed in terms of stress triaxiality.[6–10] In order to utilize such a local-fracture approach, accurate descriptions of the deformation and failure-strain/stress-triaxiality behavior of the material are necessary, with attention to the specific microstructural condition of the structural material.

In this study, we examine the sensitivity of the failure behavior of an HY-100 steel plate to stress state and inclusion content/shape, as manifested by the specimen orientation with respect to the base-plate rolling direction. Smooth and circumferentially notched tensile specimens were deformed to failure and analyzed using finite-element analysis to determine the failure conditions at the center of the specimen, where fracture initiates. The experimental approach is based on one utilized by Hancock and Mackenzie[6] and others.[7–16] Care is taken to characterize material failure by distinguishing between specimen *failure* and specimen *fracture* by using a straightforward experimental procedure. Attention is also devoted to the resulting failure behavior and its relationship to the mechanism of void coalescence. Specifically, we identify the intervention of a void-sheet mechanism, which links voids and limits failure strains at high-stress triaxialities under certain material conditions.

D.M. GOTO, formerly Graduate Student, Department of Materials Science and Engineering, The Pennsylvania State University, is Materials Engineer, Naval Surface Warfare Center, Indian Head, MD 20640. D.A. KOSS, Professor, is with the Department of Materials Science and Engineering, The Pennsylvania State University, University Park, PA 16802. V. JABLOKOV, formerly Graduate Student, Department of Materials Science and Engineering, The Pennsylvania State University, is Engineer, Siemens Westinghouse Power Corp., Orlando, FL 32826.

Manuscript submitted January 7, 1999.

II. EXPERIMENTAL AND COMPUTATIONAL PROCEDURE

A. *Material*

The material studied was HY-100 steel in the form of a commercial, hot-rolled, quenched, and tempered 25.4-mm-thick steel plate, denoted as "HY/HBO," which was provided by the Carderock Division, Naval Surface Warfare Center (NSWCCD). Table I lists the plate chemistry under the HY/HBO plate heading. Figure 1 illustrates the typical HY-100 microstructure and MnS inclusion shapes and orientations, respectively. Large MnS inclusions are elongated in the rolling direction and are somewhat lath-shaped in the rolling plane (normal to the short-transverse direction). These inclusions are, on average, 50 μm in length and possess a length-to-width aspect ratio of approximately 20:1. Quantitative metallography of approximately 100 fields of view–per-plate orientation reveals that the area fraction of large MnS inclusions (>1 μm) present is ~ 0.00015 (± 0.00005). Franklin's relationship[17] indicates, based on the Mn and S content of a steel, that the volume fraction of sulfides is roughly 0.00026, or slightly larger than the 0.00015 volume fraction measured. In addition, small (0.5 to 1.0 μm) equiaxed MnS particles, located near the larger MnS particles, are also present. In addition, irregularly shaped carbides, typically with a major dimension of 0.3 μm or less, are also present. Finally, we note that the HY-100 has a microstructurally banded structure, such that the MnS inclusions are concentrated in bands roughly 20 μm wide and spaced 50 to 60 μm apart.[18]

An additional HY-100 steel, also provided by NSWCCD, hereafter referred to as "HY/GOT" was also examined. Table I lists its respective plate chemistry. The "clean" HY/GOT material contains less sulfur than does the HY plate, as

Table I. Chemical Compositions of the HBO and GOT HY-100 Steel Plates

Wt Pct	C	Mn	P	S	Si	Ni	Cr	Mo	Cu	Ca
HY/HBO	0.16	0.26	0.008	0.009	0.22	2.62	1.32	0.25	0.14	NA*
HY/GOT	0.14	0.25	0.010	0.004	0.22	2.80	1.45	0.35	0.008	0.0043

*NA—not applicable.

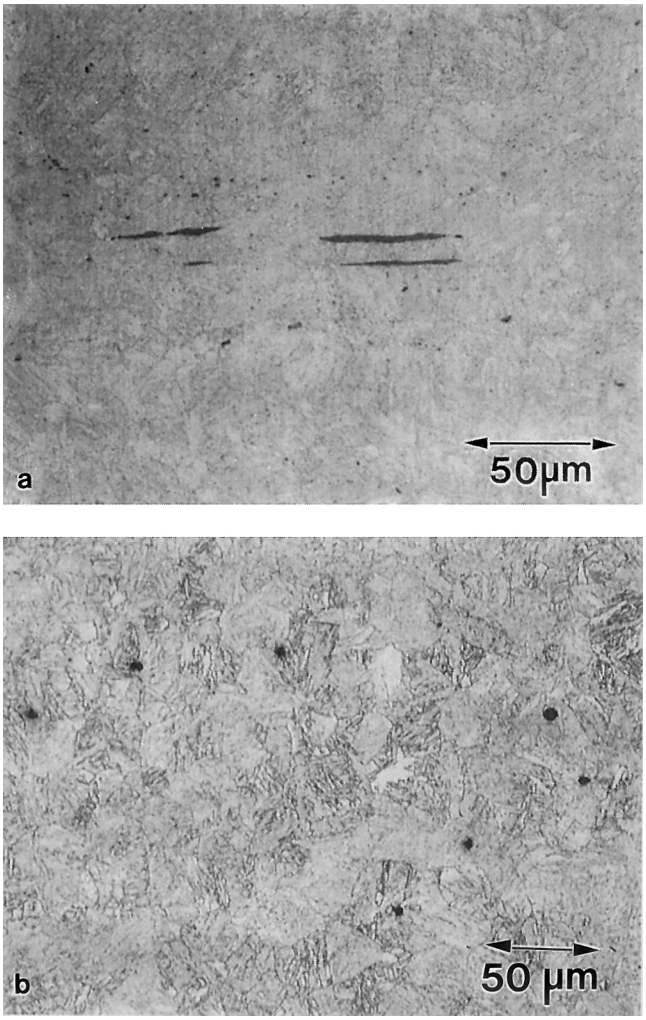

Fig. 1—Light micrographs showing inclusions in the longitudinal plane of HY-100 steel with (*a*) the HY/HBO and (*b*) the HY/GOT base metal compositions.

well as inclusion shape–control additives, *viz.*, calcium, to promote retention of spherical inclusions during hot rolling.[19] Figure 1 illustrates the markedly different inclusion morphologies between the transverse-oriented HY/HBO and HY/GOT base metals. The volume fraction of inclusions in HY/GOT ($f_{v,\mathrm{HYGOT}}$), as measured using light microscopy, was roughly 5 times that found in HY/HBO, *i.e.*, $f_{v,\mathrm{HY/GOT}} \sim 0.00080$.

B. *Specimen Design and Mechanical Testing*

The effect of triaxial tension on the failure-initiation process of the HY-100 base plate was investigated by tensile testing of smooth round-bar and circumferentially notched specimens with geometries similar to those tested by Hancock and Mackenzie.[6] Test specimens were machined from the HY/HBO and HY/GOT base-metal plates such that the applied tensile loading axis corresponded to the long-transverse plate orientation; these specimens are designated as "long-transverse" specimens. A second set of notched and un-notched round-bar tensile specimens was also machined from the HY/HBO plate, but such that the applied loading axis was oriented parallel to the plate rolling direction; these specimens are referred to as "longitudinal" specimens.

The severity of the imposed triaxial tensile stress was varied through the radius of curvature of the notch (ρ) while maintaining a constant minimum notch diameter ($2R = 7.62$ mm). Four different notch configurations were studied: $R/\rho = 0.25$, 0.5, 1.0, and 2.0. Un-notched, smooth ($R/\rho = 0.0$) tensile bars were also tested to investigate failure initiation under initial uniaxial tensile loading. For future discussion, the test bars will be referred to by plate origin and orientation and by the "R-by-ρ" ratio (R/ρ) to denote a relative indicator of triaxiality.

Notched round-bar tensile specimens were tested at 25 °C at an initial strain rate of $\approx 10^{-3}\ \mathrm{s}^{-1}$. The effective deforming "gage length" was assumed to be equal to twice the radius of curvature of the notch; finite-element analysis confirmed that most of the deformation was confined to this region. Contraction at the minimum notch diameter was monitored continuously during testing. Most of the tests were performed to specimen fracture (physical specimen separation), although some tests were interrupted as close as possible to the onset of specimen failure, prior to fracture, as will be discussed in Section III-A.

Tensile testing of smooth, un-notched test bars was performed in a manner similar to that of the notched round bars. An initial strain rate of approximately $10^{-3}\ \mathrm{s}^{-1}$ was used over a gage length of 25 mm. The gage extension was measured up to the point of necking. Once necking initiated, diametric contraction of the neck was monitored for the remainder of the test. Testing was performed both to failure initiation and fracture.

The large-strain ($\varepsilon \sim 1.0$) stress-strain response of HY-100 was determined by compression testing. These data served as the constitutive (rate-independent) response for subsequent finite-element analyses (FEA). Using a compression test procedure similar to that proposed previously,[20] cylindrical compression test specimens ($6.35 \times \phi 6.35$ mm) were tested at 25 °C at an initial strain rate of $\approx 10^{-3}\ \mathrm{s}^{-1}$. To minimize frictional effects, molybdenum disulfide lubricant and polished alumina loading platens were used. To further minimize frictional effects, testing was performed in plastic strain increments of $\Delta\varepsilon_p \sim 0.25$, up to a strain of ~ 1.0. Following each increment, the sample loading faces, as well

as platens, were relubricated. Specimens were also remachined to the original height-to-diameter ratio of 1.0 following deformation to a true strain of 0.50. The stress-strain (σ-ε) response of HY-100, as determined with the compression stress axis oriented in the long-transverse direction of the plate, is given as a power-law relationship: $\sigma = 1153\ \varepsilon^{0.089}$ (in MPa), between plastic strains of 0.002 and 1.0.

Fracture surfaces of samples strained directly to fracture were analyzed. Fractography was conducted on a limited number of tensile specimens which were initially deformed at 25 °C to a strain level corresponding to or near failure initiation and then subsequently fractured in a Charpy impact tester at −196 °C, below the ductile-to-brittle transition temperature.

C. *Finite-Element Analysis*

Finite-element analyses of the smooth and notched round-bar tensile tests were performed to estimate the local stress/strain–state conditions at failure. Specifically, the equivalent plastic strain ($\bar{\varepsilon}$) and stress triaxiality ratio ($\sigma_m/\bar{\sigma}$, where ε_m is the mean stress and $\bar{\sigma}$ is the effective stress), were calculated by the analysis at the experimentally observed load–diametric notch contraction (P-δ) condition corresponding to failure initiation. Since failure was observed to initiate at the center of the notch, the $\sigma_m/\bar{\sigma}$ and $\bar{\varepsilon}$ values were computed for this location. The $\sigma_m/\bar{\sigma}$-$\bar{\varepsilon}$ combinations which characterized failure initiation for each notch configuration were represented on a failure-limit diagram (FLD) to describe the stress state–dependent failure-initiation response of HY-100 steel.

The general-purpose ABAQUS* standard finite-element code was used to calculate local strains and stresses within the notch. Based on experimental data which showed an absence of a tension-compression strength differential and a lack of a plate-orientation effect on the compressive stress-strain response,[21] the plasticity was assumed to be isotropic, and the classical, rate-independent von Mises (J_2) flow theory was utilized. The tensile test specimen was modeled in two dimensions, taking advantage of the symmetry about the applied tensile axis and notch midplane. As such, the finite-element models are comprised of axisymmetric, four-noded quadrilateral elements (CAX4RH). The RIKS algorithm was also utilized in the analysis to provide numerical stability at large displacements, where load decreases were observed, and to terminate the simulation at a diametric (notch) contraction corresponding to that experimentally observed at the onset of failure. The constitutive material model was a "table look-up" scheme consisting of the uniaxial (large-strain compressive) stress-strain response of HY-100.

*ABAQUS is a trademark of HKS, Inc., Pawtucket, RI.

III. RESULTS AND DISCUSSION

A. *On the Definition of Failure Strains*

In this study, we define material "failure" as that condition in which material damage is sufficiently severe as to measurably degrade the material's stress-carrying capacity with increasing deformation. Material failure is identified using an experimental procedure depicted in Figure 2, in which the loss of stress-carrying capacity of the material due to internal damage is separated from that due to specimen necking. As illustrated by this figure, specimen necking results in a continuously decreasing load-displacement response which is characterized by a gradually increasing value of $-dP/d\delta$, where P is the load and δ is the specimen displacement. However, at material failure, an additional loss of load-carrying capacity due to material damage is manifested by a detectable increase in $-dP/d\delta$. The onset of this increase in specimen "compliance" marks failure initiation, in our definition. The acceleration of the load loss following failure initiation also indicates that material damage is sufficiently severe, such that damage evolution is "self-sustaining" with further deformation.

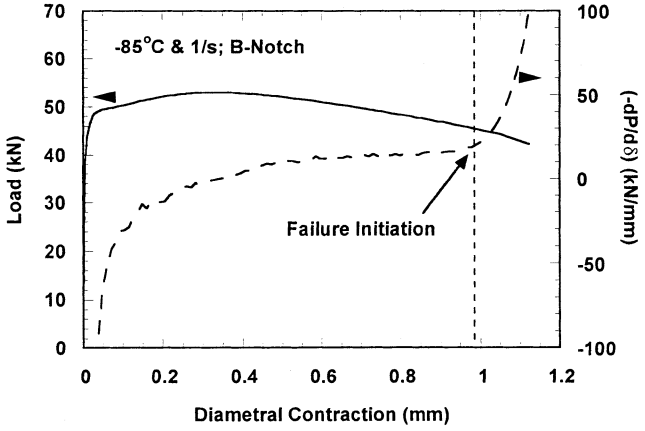

Fig. 2—The load and specimen compliance response as a function of diametric contraction of a $R/\rho = 0.5$ notched tensile specimen (solid line). Failure initiation is identified by the rapid change in specimen compliance (dashed line).

Failure is tantamount to roughly a 2 pct load loss based on the load-displacement response of the specimens, suggesting an ≈2 pct loss of load-bearing area due to damage accumulation. Ultrasonic C-scan imaging and metallography sectioning indicate that this damage, in the form of microvoids, is present at failure and concentrates near the symmetry axis of the specimen, with the highest concentration of voids located in the centermost region of the notch, where the stress-triaxiality level is most severe. Quantitative fractography of interrupted/liquid nitrogen–fractured specimens indicates that, at failure initiation, approximately 3 pct of the projected fracture surface, *viz.*, at the center of the surface, is characterized by ductile microvoids. In this latter testing scheme, specimens initially deformed to failure at room temperature are subsequently "V notched" and fractured at −196 °C. The undamaged steel section is fractured in a brittle manner by cleavage, thus allowing identification of the previously accumulated ductile microvoids. These observations indicate that our definition of failure is characterized by damage accumulation in the form of microvoid fracture, which concentrates in the center of the notched section and which accounts for roughly a 2 to 3 pct loss of load-bearing material.

Our definition of failure strain, based on initial and final diameter, differs from that of conventional fracture strain in that it represents the failure-initiation process prior to

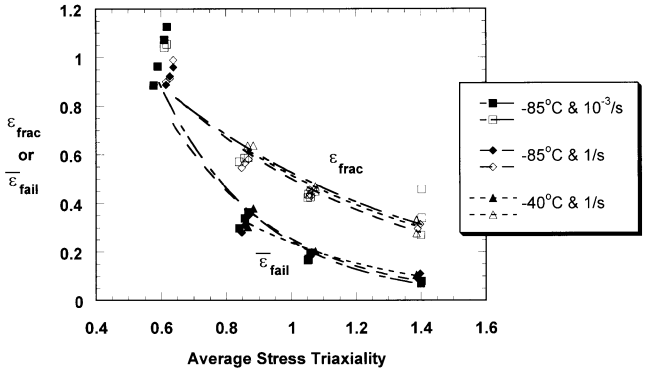

Fig. 3—The dependence of fracture strain and failure strain on the average stress triaxiality for notched and un-notched HY/HBO tensile specimens tested to fracture.

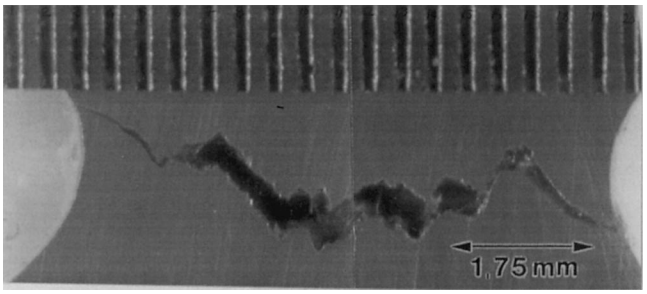

Fig. 4—A light micrograph showing the profile of a fractured $R/\rho = 2.0$ notched HY/HBO tensile specimen with the applied tensile axis parallel to the long transverse plate orientation.

subsequent crack-growth/shear lip/cup-cone formation in these tensile specimens. Figure 3 illustrates the difference between failure strain and fracture strain, based on a large number of cryogenic tests of transverse-oriented HY/HBO material. These data, as well as those of an HSLA-100 steel tested at room temperature,[20] show that the *fracture* strains are roughly a factor of 2 larger than the *failure* strains at high-stress triaxialities, *i.e.*, $\ln(d_{fract}/d_0) \approx 2\ln(d_{fail}/d_0)$. It should be noted that, with the exception of the cryogenic, intermediate $\sigma_m/\overline{\sigma} \approx 0.85$ condition, the cryogenic failure strains of the HY/HBO material are similar to those observed in this study at room temperature. Finally, we note that in both the HY/HBO and HSLA steels, the fracture and failure strains appear to converge for the (initially) uniaxial test condition.

The behavior shown in Figure 3 is a result of failure initiation at the specimen center, where the stress triaxiality is large, and subsequent crack propagation/shear lip formation under decreasing stress triaxiality as fracture progresses to the specimen surface. The latter crack growth results in a considerable amount of additional diametric notch contraction, making a specimen fracture strain, calculated from initial and final specimen diameters, much larger than a comparable local strain-to-fracture within the specimen/notch center. This effect is evident in Figure 4, which shows that significant fracture-surface separation occurred near the center of the specimen, where failure initiated, by the time the specimen fractured due to shear lip formation. Also noticeable in this figure is the zigzag nature of the fracture surface in the profile view of this $R/\rho = 2.0$ notched, high-stress-triaxiality specimen. We shall return to this issue later in Section III-C.

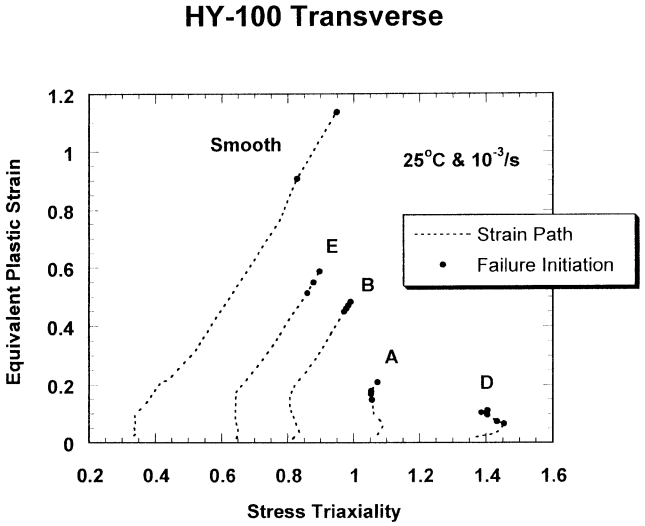

Fig. 5—The strain paths experienced by a finite element at the center of the notch of HY/HBO tensile specimens (long transverse orientation) possessing notch acuities between $R/\rho = 0$ and 2.0.

B. *Failure-Limit Diagram Behavior*

Given the previous definition of material failure and the physical location of the failure-initiation process, we utilized FEA to describe the multiaxial stress state and equivalent plastic strain at the center of the notch. Based on the finite-element results, an FLD is generated to express the combinations of stress triaxiality and equivalent plastic strain ($\sigma_m/\overline{\sigma} - \overline{\varepsilon}$) which result in failure.

One difficulty with the construction of an FLD is the range of stress triaxialities that can develop within the specimen during deformation to failure. For example, Figure 5 shows stress-triaxiality histories from initial deformation to failure of the HY-100 steel. While this range of triaxiality values is comparatively small for the notched specimens, the initially uniaxial smooth-bar specimen is subjected to a large variation of stress triaxiality from 0.33 to about 0.95. The implication of this large interval in stress-triaxiality evolution is in its effect on damage evolution and, therefore, failure. Material failure is a consequence of damage evolution, which is quite sensitive to stress triaxiality. For example, we expect damage accumulation in the smooth tensile bar initially to occur slowly at small strains (at low-stress triaxialities) but to accelerate with deformation, in part due to increasing stress triaxiality as necking occurs. The failure strains illustrated in Figure 3 for the smooth tensile bar can, therefore, be interpreted as resulting from damage accumulating over a relatively large stress-triaxiality interval (between $\sigma_m/\overline{\sigma} = 0.33$ and 0.95). This accumulation of damage over a relatively large triaxiality interval serves as a warning of the difficulty of analyzing commonly employed uniaxial tensile test data in addressing ductile damage accumulation behavior in metals.

In view of this, we have constructed a failure-limit diagram of multiaxially loaded HY-100 steel by employing an *average* stress-triaxiality ratio over the strain interval, defined as follows:

$$(\sigma_m/\overline{\sigma})_{\text{ave}} = \frac{\int (\sigma_m/\overline{\sigma})\, d\overline{\varepsilon}}{\int d\overline{\varepsilon}} \qquad [1]$$

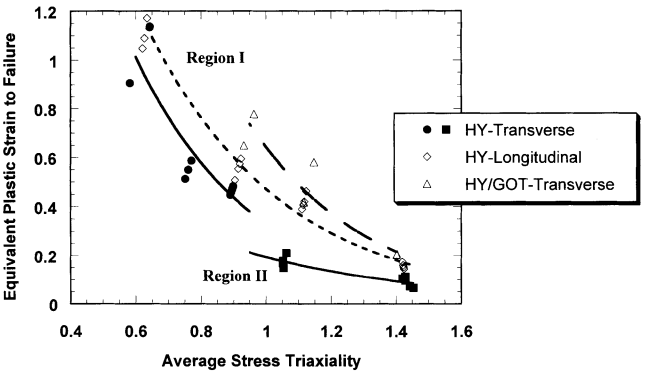

Fig. 6—An FLD illustrating region I and II failure behavior for HY-100 steel with the "conventional" HY/HBO as well as the Ca-modified HY/GOT composition.

In effect, we imply that failure is a consequence of damage accumulating at an average rate dictated by the average stress triaxiality. While not ideal, this procedure seems to us more representative of the imposed stress state than simply using the final stress-triaxiality condition at failure, as has typically been done in the past.[6–16] Much of the rationale for this decision relies on extensive damage data for this steel,[22] which shows that the strain-induced damage accumulation (*i.e.*, void volume fraction and void density) increase rapidly with increasing stress triaxiality. Thus, it seems more appropriate to identify failure of a particular specimen with the *average* rather than a *final* stress triaxiality; hence, Eq. [1]. Finally, it should be recognized that the data in Figure 5 indicate the difference between the average stress-triaxiality value (as expressed in Eq. [1]), and the final triaxiality value is relatively small for the notched tensile specimens; it is large only for the smooth bar specimens.

The FLD for the HY/HBO base-plate material, tested in the long-transverse and longitudinal orientations, and the HY/GOT material, tested long transversely, is shown in Figure 6. The failure data correspond to $\sigma_m/\overline{\sigma} - \overline{\varepsilon}$ combinations at the center of each notch, where failure is observed to initiate. As expected from previous studies,[6–16] the FLD indicates that strain to failure rapidly decreases as the severity of triaxial tension increases. However, there are several differences in the failure behavior among the materials, and these are described subsequently.

As shown in Figure 6, plate chemistry can significantly improve the failure-initiation resistance, particularly at lower stress-triaxiality levels, *cf.*, the failure strains of the "cleaner" HY/GOT plate material to that of the similarly long transverse–oriented conventional HY/HBO material. The decrease in sulfur level and the addition of Ca to promote retention of spherical inclusions clearly has a beneficial effect in improving fracture resistance. The beneficial effect is pronounced when the transversely oriented specimens are compared, although the Ca-treated transverse material has only somewhat higher failure strains than the longitudinal HY/HBO plate (Figure 6).

Specimen orientation also has a significant effect on failure, as indicated in Figure 6. As expected from the presence of large elongated MnS stringers parallel to the rolling direction, the fracture resistance of the longitudinally oriented (with respect to the rolling direction) specimens is significantly higher than in those specimens having the long-transverse orientation.

However, somewhat unexpected is the FLD behavior of the HY/HBO steel tested in the long-transverse plate orientation. The failure data, shown in Figure 6, suggest that two distinctly different dependencies of the failure strain ($\overline{\varepsilon}$) on imposed stress triaxiality exist, with a transition occurring at a $\sigma_m/\overline{\sigma}$ value of approximately 1.05. Thus, we separate the FLD behavior of the HY/HBO long-transverse material into two regions, referred to as regions I and II, respectively. The implication of separation of the failure behavior is that two differing ductile failure-initiation mechanisms operate in this plate orientation, and that these two mechanisms depend differently on the imposed stress-triaxiality level. Region I failure behavior exists at lower stress-triaxiality levels, from test results of smooth ($R/\rho = 0.0$), E-notch ($R/\rho = 0.5$), and B-notch ($R/\rho = 1.0$) specimen geometries, and is manifested by rapidly decreasing failure strains which are sensitive to small changes in the imposed stress triaxiality. Region II behavior also appears to be present only in the HY/HBO failed at the highest triaxiality levels, *i.e.*, the A-notch ($R/\rho = 1.0$) and D-notch ($R/\rho = 2.0$) configurations. In contrast to region I failure behavior, region II failure is characterized by small failure strains that appear to be much less sensitive to imposed stress triaxiality.

The failure strain results in Figure 6 also suggest that region I appears to characterize the FLD behavior of both the longitudinal HY/HBO as well as the HY/GOT material (which was tested in the long-transverse plate orientation). The absence of a readily discernable discontinuity in the failure strain–stress-triaxiality response suggests that region I behavior exists over the entire range of stress triaxialities investigated by this study. The fracture surface observations, discussed in the following section, address the differences between region I and II failure-initiation behavior.

Finally, we note that all the FLD data appear to converge with increasing stress triaxiality (Figure 6). For example, the differences in failure strains at high $\sigma_m/\overline{\sigma}$ levels, *e.g.*, characteristic of the $R/\rho = 2.0$ notch, between the clean HY/GOT plate and those of the longitudinal HY/HBO plate, are small. Nevertheless, these latter failure-strain values are still at least 50 pct greater than the "small" values characteristic of the long transverse–oriented HY/HBO steel at these triaxialities.

C. *Fractography and Failure Mechanisms*

The FLD behavior suggests the presence of two controlling failure mechanisms active in long transverse–oriented HY/HBO HY-100 steel. Since no evidence of cleavage (brittle) fracture was found, ductile fracture processes dictate failure. Consistent with this hypothesis and with the behavior suggested by the FLD data (Figure 6), the fractography of the *long transverse*–oriented HY/HBO steel base-plate specimens, as shown in Figures 7 and 8, indicates that two different void coalescence (and possibly nucleation) mechanisms control failure in regions I and II. Region I ($\sigma_m/\overline{\sigma} <$ 1.05) fracture is characterized by surfaces which exhibit relatively equiaxed voids which have grown and coalesced by impingement (Figure 7(a)). As is common in ductile microvoid fracture, the fracture surface assumes an irregular topology and involves a significant volume of deforming

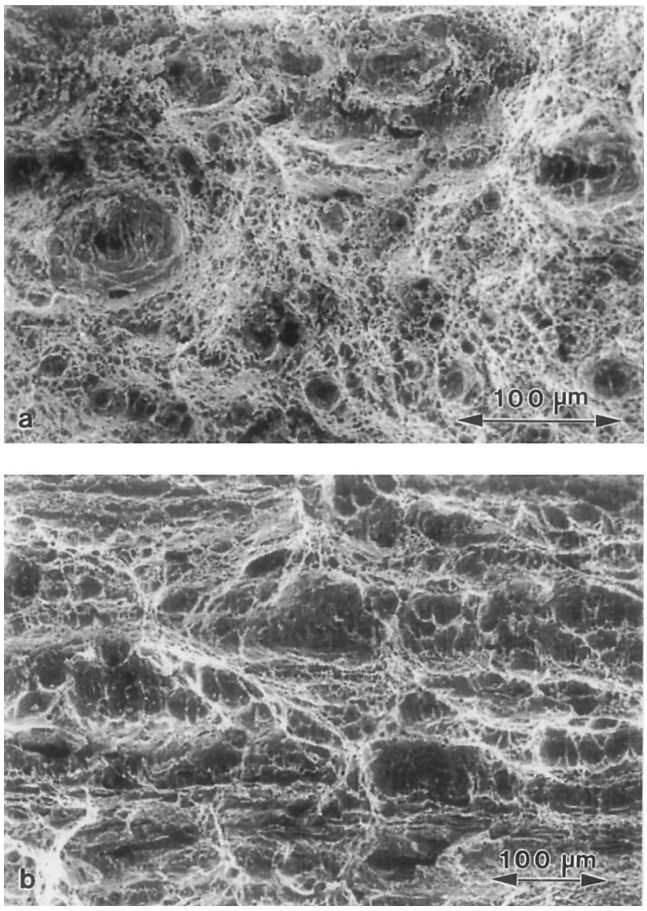

Fig. 7—Fractography of D-notched ($R/\rho = 2.0$) tensile specimens oriented in the long transverse direction of the plate for the (*a*) HY/GOT and (*b*) HY/HBO compositions.

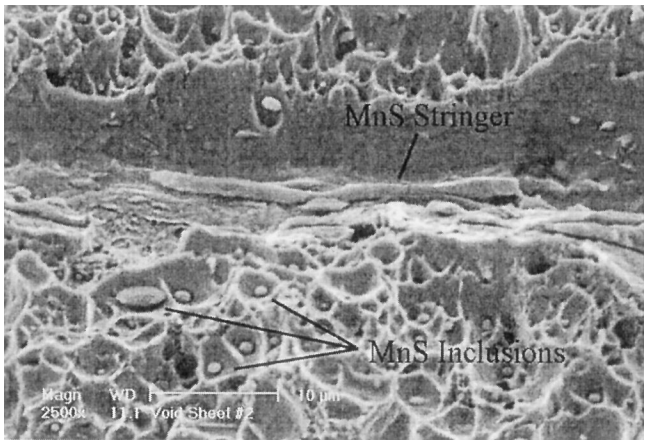

Fig. 8—A fractograph from a void-sheet failure surface showing an elongated MnS stringer surrounded by equiaxed dimples containing fine-scale MnS particles.

material. A few neighboring voids within this volume grow to a large size and impinge. We denote this form of failure as being void coalescence due to impingement of "global damage." Global damage is employed to described the voids participating in fracture, as they appear to be distributed over a relatively large volume of material and are not localized onto a plane.

In contrast to equiaxed voids growing to impingement, the fracture surfaces shown in Figures 7(b) and 8, corresponding to failure within region II ($\sigma_m/\overline{\sigma} > 1.05$) of the long transverse–oriented HY-100, are characterized by a *void-sheet failure*.[23,24,25] Large, elongated, primary voids are linked by a "zigzag" arrangement of planes, which are inclined at ≈45 deg with respect to the maximum principal stress axis; *cf.*, Figure 4. The inclined "void-sheet" planes are covered by small, equiaxed microvoids nucleated at small (approximately 1 to 2 μm) equiaxed MnS inclusions concentrated near the large, elongated inclusions (Figure 8) and even smaller (0.1 to 0.3 μm) particles, presumably carbides, near the midpoint between the large inclusions.

The large elongated voids are aligned (parallel to the rolling direction) and are present at different elevations on the fracture surface, thus giving rise to an alternating ridge-trough or layered fracture-surface appearance. These aligned elongated voids are associated with the elongated MnS inclusion or, more often, with a stringer of elongated MnS inclusions, as shown in Figure 8. The large elongated voids vary in length between 150 and 700 μm and have an average length-to-width ratio of 7:1. Although the void lengths are markedly larger than the lengths of individual, elongated MnS inclusions (~15 to ~75 μm), the former lengths are consistent with clusters or stringers of elongated MnS inclusions. During deformation, these inclusions debond and/or fracture, initiating an elongated void. The average intervoid spacing (actual) between adjacent elongated MnS inclusion-nucleated voids on neighboring "ridges" or "troughs" is ≈70 μm. This separation distance is consistent with an observed chemical banding wavelength of ≈50 μm. Finite-element modeling[26] indicates that the presence of these 45 deg inclined planes, linking neighboring ($\Delta = 70$ μm), elongated inclusion-nucleated voids, is consistent with void-sheet linking by a localized shear instability failure of the intervoid steel matrix between the elongated MnS inclusion-nucleated voids.

The longitudinally oriented HY/HBO and the HY/GOT long-transverse HY-100 steels do *not* exhibit elongated voids or a layered/ridge-trough fracture surface morphology. Equiaxed, ductile "dimpled" microvoid features are observed on all specimens fractured over the entire range of investigated stress-triaxiality levels, which is consistent with void coalescence by impingement. Equiaxed voids found on HY/GOT fracture surfaces are generally hemispherical in shape and are separated from their neighbors by a narrow ligament of material (thinned down to a knife-edge). Also, found at the base of many voids are small spherical (1 to 2 μm diameter) particles. Although no attempt was made to identify the elemental make-up of these inclusions, it is likely that they contain Mn, S, and/or Ca. Thus, we conclude that failure of the HY/HBO longitudinal, as well as of the HY/GOT long-transverse steels, is also controlled by a process similar to that at low-stress triaxialities in the HY/HBO long-transverse case: global damage accumulation in which void coalesence occurs by void impingement.

D. *The Dependence of Failure on Stress Triaxiality*

1. *Region I of the FLD*

Our experimental observations indicate that failure initiation in these HY-100 steels shows a strong sensitivity to stress state, especially within region I of the FLD, where

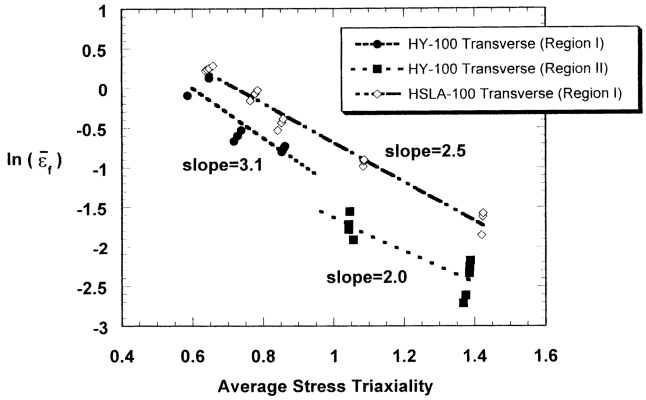

Fig. 9—The dependence of the equivalent strain at failure on average stress triaxiality for HY-100 steel with either the HY/HBO or HY/GOT composition and tested in either the long transverse or longitudinal orientation of the base plate.

void coalescence by impingement and global damage accumulation dictate failure. We know that such failure occurs as a result of the damage accumulation caused by the nucleation, growth, and linking of voids. We believe that the larger voids are associated with either equiaxed or elongated sulfide particles, which we know initiate voids at small strains (<0.05).[22] The presence of voids at small strain levels, even at low-stress triaxialities, suggests that the stress-state dependence of the failure strain originates from the void growth and/or void coalescence process.

If void growth behavior is critical to the failure of these steels, then we might expect a Rice–Tracey[27]-like dependence of failure strains to imposed stress triaxiality. This possibility was recognized by Hancock and Mackenzie,[6] who, in analyzing the FLD of two high-strength low-alloy steels, proposed that

$$\bar{\varepsilon}|_{\text{fail}} = \alpha \exp\left(-\beta\sigma_m/\bar{\sigma}\right) \qquad [2]$$

where $\bar{\varepsilon}|_{\text{fail}}$ is the failure strain, α is a material constant, and β is a constant whose value should be approximately 1.5 if the voids grow in an isolated, noninteracting manner, as initially analyzed by Rice and Tracey[27] and others.[28] It should also be recognized that Eq. [2] implies a failure criterion based on either a critical void growth rate or critical void volume fraction, if neither is dependent on stress triaxiality.

Figure 9 shows that the failure strains do obey an exponential relationship with stress triaxiality, analogous to that given by Eq. [2]. However, for region I failure behavior, the value of the pre-exponential factor (β) ranges from 2.5 to 3.1. In other words, the dependence of the failure strains on stress triaxiality is stronger than that expected from a Rice–Tracey failure criterion ($\beta = 1.5$) for a failure process dominated by void growth and due to void coalescence by impingement. This strong dependence may be due to several factors. As mentioned previously, if failure obeyed a critical void-volume fraction criterion, then a β value in excess of 1.5 would be expected *if* the critical void fraction itself decreased with increasing stress triaxiality, as might be expected.[15,29,30] Alternatively, void interactions which increase in severity with increasing triaxiality would also act to decrease the failure strain at high triaxialities, resulting in an increase in the exponential factor; this effect might also be expected in view of computational modeling of void growth behavior.[31] Finally, the rate of damage initiation is expected to increase with increasing triaxiality for those voids in need of the nucleation strain, such as the carbide-initiated voids.[24,25] All of these possibilities are likely, although the small level of inclusions present in the steel (volume fraction $\approx$0.00015) suggests large intervoid spacings ($>>$10 void diameters), so that void interactions should be minimal.

2. *Region II of the FLD*

At high stress triaxialities, the failure in HY/HBO steel in the long-transverse orientation results in region II behavior of the FLD. Reiterating, region II behavior is characterized by small failure strains and a weaker sensitivity of the strain to failure on stress triaxiality, such that $\beta \approx 2.0$. Failure under these conditions initiates by void-sheet linking of a small volume fraction (volume fraction $\approx$0.00015) of inclusions, dominated by neighboring, elongated MnS inclusion-nucleated voids oriented normal to the principal tensile direction. This void microstructure suggests a modeling approach involving circular holes whose growth and linking cause failure,[26] akin to that initially proposed by McClintock.[32] If failure were limited by hole growth, rather than by growth of initially spherical voids, the exponential factor in Eq. [2] should have a value of 1.6 to 1.7,[32] which is, in fact, relatively close to the 2.0 value observed in Figure 9. Such an interpretation suggests that the void sheet/shear instability, which we believe controls region II failure, obeys some form of a critical hole-growth criterion for failure; this issue is addressed subsequently.

As has been modeled using finite element analysis,[26] the presence of elongated primary voids in the form of 2.5-μm-diameter circular voids, spaced 70 μm apart on a 45 deg plane (which models the fractography), can induce void-sheet failure, but *only* at high-stress triaxialities.[26] The sensitivity of the onset of the void-sheet localization event to stress triaxiality is also predicted by the FEA, such that increasing triaxiality decreases the far-field strain necessary to develop void-sheet failure. As hypothesized previously, the similar β values in Eq. [2] for McClintock hole growth and experimental failure strains suggests a hole-growth criterion for the onset of void-sheet failure. Interestingly, the computational results *support* such a hypothesis. An examination of the predicted values of the hole sizes at the onset of the intervoid shear instability indicate that, for three different stress triaxialities (which span our experimental ranges), the shear instability always develops at hole sizes in the 15 to 20 μm ranges.[33]

Finally, in the previous finite-element model,[26] at failure, the holes have grown considerably, from 2.5 to 15 to 20 μm, but are still spaced roughly 60 μm apart. Thus, void linking occurs when voids grow to approximately one-third of the intervoid spacing. Such a criterion differs by a factor of approximately 3 from the void coalescence criterion, which states that (initially spherical) voids coalesce by impingement when they grow to a major dimension, such that their length is roughly equal to their spacing.[34] In other words, if voids can develop into holes, void linking and specimen failure can occur at comparatively large void spacings. Thus, region II void-sheet failure can be expected to intervene at high stress triaxialities, even at small inclusion contents, provided the inclusion-initiated voids are elongated (*i.e.*, behave like holes) and oriented normal to the stress axis.

IV. SUMMARY

Depending on specimen orientation, the failure behavior of a hot-rolled "conventional" HY-100 base plate, denoted HY/HBO, can be dominated by two distinct failure-initiation mechanisms that depend on imposed stress triaxiality and are represented by a two-region FLD (regions I and II). *Region 1* behavior is characterized by larger failure strains and exhibits a strong inverse exponential dependence of the failure strain on increasing stress triaxiality. Damage accumulation, in which relatively equiaxed voids coalesce by growing to impingement, describes the dominant ductile fracture process in this region. For the conventional HY-100 base plate (HY/HBO) with MnS inclusions elongated in the rolling direction, region I behavior is observed only at low-to-intermediate–stress triaxilities ($\sigma_m/\overline{\sigma} < 1.05$) in specimens oriented in the long-transverse orientation of the plate. In contrast, region I failure occurred at all stress-triaxiality levels for material loaded along the plate's rolling direction. *Region II* behavior imposes the limited ductility of the HY/HBO plate at high levels of applied stress triaxiality ($\sigma_m/\overline{\sigma} > 1.05$) when specimens are oriented in the long-transverse plate orientation. This region is characterized by small failure strains, which exhibit a weaker sensitivity to stress triaxiality than region I failure. Failure initiation in this case occurs by a void-sheet instability process, in which elongated MnS-initiated voids trigger deformation localization within the intervoid ligament.

Region I–type failure occurs over the entire stress-triaxiality interval investigated in the lower-sulfur and calcium-treated HY/GOT steel base plate. When compared to the conventional HY-100 specimens oriented in the same long-transverse direction of the plate, the HY/GOT material shows an increased resistance to failure initiation, particularly at intermediate-stress triaxialities. This increase in ductility is primarily due to the suppression of the local conditions which cause void-sheet failure. However, the failure-initiation behavior of the HY/HBO and HY/GOT materials tends to converge at high triaxiality levels, suggesting that improvements in failure resistance through the use of inclusion shape control and "cleaner" plate chemistry diminish at high-stress triaxialities.

Failure strains within both regions of the FLD obey an exponential relationship with stress triaxiality, as would be expected if void growth is a dominant factor in controlling failure. However, the strong dependence of the region I failure strains on stress triaxiality results in relatively large values of the exponential factor (2.5 to 3.1 in the current study, as opposed to that of 1.5 predicted by a Rice–Tracey analysis[27]). Thus, while the growth of isolated voids is an important factor in determining failure, other factors such as matrix plasticity, spatial distribution of voids/inclusions, and void interaction effects must also be considered when failure occurs by coalescence of voids due to impingement. On the other hand, the region II failure data (void sheet) appear to obey a failure criterion based on hole growth and are consistent with the implications of a previous computational model[26] of the void-sheet failure mode, which controls region II failure in the transverse-loaded HY-100 steel with a conventional chemistry.

ACKNOWLEDGMENTS

This research was supported by the Office of Naval Research and by the Naval Surface Warfare Center. Comments and discussions with D. Chae, J. Bandstra, C. Young, R. Garrett, J. McKirgan, E. Czyryca, A. Geltmacher, P. Matic, and R. Everett are gratefully acknowledged.

REFERENCES

1. D.M. Norris, J.E. Reaugh, B. Moran, and D.F. Quinones: *J. Eng. Mater. Technol.*, 1978, vol. 100, pp. 279-86.
2. A. Pineau: *Proc. 5th Int. Conf. on Fracture*, D. Francois, ed., Pergamon Press, Elmsford, NY, 1981, vol. 2, pp. 533-77.
3. F.M. Beremin: *Metall. Trans. A*, 1983, vol. 14A, pp. 2277-87.
4. G. Rousselier: *Nucl. Eng. Design*, 1987, vol. 105, pp. 97-111.
5. J. LeMaitre: *Eng. Frat. Mech.*, 1986, vol. 25, pp. 523-37.
6. J.W. Hancock and A.C. MacKenzie: *J. Mech. Phys. Solids*, 1976, vol. 24, pp. 147-69.
7. A.D. MacKenzie, J.W. Hancock, and D.K. Brown: *Eng. Fract. Mech.*, 1977, vol. 9, pp. 167-88.
8. J.W. Hancock and D.K. Brown: *J. Mech. Phys. Solids*, 1983, vol. 31, pp. 1-24.
9. J.W. Hancock and R.D. Thomson: *Mater. Sci. Technol.*, 1985, vol. 1, pp. 684-90.
10. G.R. Johnson and W.H. Cook: *Eng. Fract. Mech.*, 1985, vol. 21, pp. 31-48.
11. B. Marini, F. Mudry, and A. Pineau: *Eng. Fract. Mech.*, 1985, vol. 22, pp. 989-96.
12. R. Batisse, M. Bethmont, G. Devesa, and G. Rouseelier: *Nucl. Eng. Design*, 1987, vol. 105, pp. 113-20.
13. S. Jun: *Eng. Fract. Mech.*, 1991, vol. 39, pp. 799-805.
14. R. Becker, A. Needleman, O. Richmond, and V. Tvergaard: *J. Mech. Phys. Solids*, 1988, vol. 36, pp. 317-51.
15. T. Pardoen, I. Doghri, and R. Delannay: *Acta Mater.*, 1998, vol. 46, pp. 541-52.
16. T. Pardoen and F. Delannay: *Metall. Mater Trans. A*, 1998, vol. 29A, pp. 1895-1909.
17. A.G. Franklin: *J. Iron Steel Inst.*, 1969, vol. 207, pp. 181-86.
18. D. Chae: The Pennsylvania State University, University Park, PA, unpublished research, 1998.
19. A.D. Wilson: in *Inclusion and Their Influence on Material Behavior*, R. Rungta, ed., ASM INTERNATIONAL, Materials Park, OH, 1989, pp. 21-34.
20. M.L. Lovato and M.G. Stout: *Metall. Trans. A*, 1992, vol. 23A, pp. 935-51.
21. D. Goto: The Pennsylvania State University, University Park, PA, unpublished research, 1998.
22. V. Jablokov: M.S. Thesis, The Pennsylvania State University, University Park, PA, 1998.
23. T.B. Cox and J.R. Low: *Metall. Trans.*, 1974, vol. 5, pp. 1457-70.
24. R.H. Van Stone, T.B. Cox, J.R. Low, and J.A. Psioda: *Int. Met. Rev.*, 1985, vol. 30, pp. 157-79.
25. W.M. Garrison and N.R. Moody: *J. Phys. Chem. Solids*, 1987, vol. 48, pp. 1035-74.
26. J.P. Bandstra, D.M. Goto, and D.A. Koss: *Mater. Sci. Eng. A*, 1998, vol. A249, pp. 46-54.
27. J.R. Rice and D.M. Tracey: *J. Mech. Phys. Solids*, 1969, vol. 17, pp. 201-17.
28. M.J. Worswick and R. Pick: *J. Mech. Phys. Solids*, 1990, vol. 38, pp. 601-25.
29. R. Becker: *J. Mech. Phys. Solids*, 1987, vol. 35, pp. 577-99.
30. P.F. Thomason: *Acta Metall.*, 1985, vol. 33, pp. 1079-85 and 1087-95.
31. C.L. Hom and R.M. McMeeking: *J. Appl. Mech.*, 1989, vol. 56, pp. 309-17.
32. F.A. McClintock: *J. Appl. Mech., Trans. ASME*, 1968, vol. 90, pp. 363-71.
33. J.P. Bandstra: The University of Pittsburgh at Johnstown, private communication, 1998.
34. L.M. Brown and J.D. Embury: *Proc. 3rd Int. Conf. on Strength of Metals and Alloys*, Institute of Metals, London, 1973, pp. 164-69.